CrystEngComm

ROYAL SOCIETY OF CHEMISTRY

COMMUNICATION

View Article Online
View Journal | View Issue

Cite this: *CrystEngComm*, 2024, **26**, 2746

Received 7th April 2024,
Accepted 30th April 2024

DOI: 10.1039/d4ce00338a

rsc.li/crystengcomm

Facile synthesis of a 2,5-dihydroxyterephthalic acid-based charge transfer cocrystal for photoelectric applications†

Pei-Pei Yin,[ab] Yu-E Chen,[b] Jia-Wei Diao,[b] Yi-Yang Cheng,[b] Xiao-Gang Yang,[*b] Bao-Zhong Liu*[a] and Lu-Fang Ma[ab]

Herein, a 2,5-dihydroxyterephthalic acid-based cocrystal complex was facilely synthesized using a mixture of ethanolic solutions of the two coformers under a few minutes at room temperature. The high photocurrent ratio of 712 between the illumination and dark states and the successful fabrication of a phosphor-converted light-emitting diode device make this cocrystal complex a promising candidate in fields of photoelectric detectors and solid-state lighting.

The development of charge transfer materials has drawn ever-increasing attention towards solar cells, field effect transistors, photodetectors, photocatalysis, and organic light-emitting diodes (OLEDs) and so on.[1–6] Charge transfer would cause the orbital hybridization between the highest occupied molecular orbital of the donor and the lowest unoccupied molecular orbital of the acceptor, resulting in more appealing physicochemical properties.[7,8] In this context, co-crystalline engineering driven by non-covalent interactions such as hydrogen bonds, halogen bonds, electrostatic and π–π stacking interactions between the donor and acceptor (D–A) has been proven as a promising and effective approach to obtain novel and unpredicted physicochemical properties by the synergistic and collected effects.[9–17]

In comparison with the covalent synthesis of large molecular arrays, organic cocrystal complexes exhibit many merits of low cost, facile synthesis, large scale, low defect, and uniform morphology.[18] The strategy of functional integration endows the cocrystal materials with tunable band gap, adjustable molecular arrangement and easy functionality.[19,20] Wang's group reported that the yellow emission of 1,4-bis(4-cyanostyryl)benzene (*p*-BCB) can be tuned to sky-blue by the introduction of 1,4-diiodo tetrafluorobenzene through cocrystal engineering.[21] Assembled with three typical isophthalic acid derivatives, our group obtained acridine-based cocrystal complexes with adjustable energy levels, a wide range of photoluminescence color (UV to orange), and rotational angle-dependent polarized emission. In addition, the fabrication of orderly and uniform cocrystal thin films further presents tunable one-/two-photon up-conversion and efficient mobility and separation of electron–hole pairs.[22] Recently, thermally-activated delayed fluorescence (TADF) was observed by Hu's group in the charge transfer cocrystal of *trans*-1,2-diphenylethylene (TSB) and 1,2,4,5-tetracyanobenzene (TCNB). They stated that the intermolecular charge transfer of TSB–TCNB narrows the singlet–triplet energy gap, and therefore, facilitates reverse intersystem crossing for TADF.[23] To date, despite achieving prominent progress in cocrystal engineering, the rational design and selection of donor/acceptor components and exploration of internal D–A interaction mechanisms still restrict the practical applications of cocrystal materials.

Generally, the efficiency of charge transfer greatly depends on the ionization potential of the donor, electron affinity of the acceptor, and electrostatic coulombic interaction in the complex. The degree of wave-function overlap between D–A has a great influence on the optoelectronic and OLED applications of cocrystals. Herein, 2,5-dihydroxyterephthalic acid (DTPA) was selected as the electron donor by the consideration of its constitutional stiffness and four pH-dependent abstractable protons.[24] Meanwhile, as a type of outstanding organic chromophore linker, DTPA has been used to construct metal–organic frameworks (MOFs) with tunable fluorescent emission.[25–27] In contrast, DTPA-based cocrystal complexes have rarely been studied. In this work, we report the synthesis, crystal structure and detailed

[a] *College of Chemistry and Chemical Engineering, Henan Polytechnic University, Jiaozuo, 454000, P. R. China. E-mail: bzliu@hpu.edu.cn*
[b] *College of Chemistry and Chemical Engineering, Luoyang Normal University, Henan Province Function-Oriented Porous Materials Key Laboratory, Luoyang 471934, P. R. China. E-mail: yxg2233@126.com*

† Electronic supplementary information (ESI) available: Experimental details and structure data table, PXRD, crystal structures and photoluminescent spectra. CCDC 2340776. For ESI and crystallographic data in CIF or other electronic format see DOI: https://doi.org/10.1039/d4ce00338a

photophysical properties of the DTPA-based cocrystal prepared by the introduction of the electron acceptor 1,10-phenanthroline (Phen). The heteroaromatic coformer Phen has a conjugated rigid planar structure, which can capture protons from the carboxylic group of DTPA. The title cocrystal Phen–DTPA can be facilely and immediately synthesized by the mixture of DTPA and Phen ethanol solution in a few minutes at room temperature (Scheme 1). It shows an alternative DADA stacking mode at the molecular level with a sufficient D–A π-electron overlap, which was fixed by strong hydrogen bonds, charge transfer and π–π stacking interactions in a rigid environment. This work not only provides a facile and scale-up method for the synthesis of 2,5-dihydroxyterephthalic acid-based charge transfer cocrystals but also extends its application in photoelectric detectors and phosphor-converted light-emitting diodes.

To understand the donor–acceptor interactions in the formation of cocrystals, fluorescence (FL) spectra of DTPA in ethanol (5×10^{-4} M) with the gradual addition titration of Phen ethanol solution (5×10^{-4} M) were measured (λ_{ex} = 380 nm). It can be seen from the FL spectra that the main emission peak at 450 nm attributed to DTPA increased initially (Fig. 1a) and then decreased gradually (Fig. 1b) with the addition of Phen. At the same time, a weak shoulder peak around 510 nm could also be detected, which has been enhancing gradually throughout the process, and then became a main emission peak. While the peak at 450 nm turned into a weak shoulder one. The inserts in Fig. 1 show a significant emission color change of DTPA ethanol solution from intense cyan to green before and after the addition of Phen. The final FL spectrum is similar to that of the Phen–DTPA cocrystals dispersed in ethanol (Fig. S1†). From the above observation, it can be speculated that the self-assembly of the Phen–DTPA cocrystal involves two processes: red shifts and enhancement of the emission spectra originating from the π → π* electronic transition between DTPA molecules, charge transfer between DTPA and Phen-induced partial fluorescence quenching. Generally, the former is favorable for optical materials applied in OLEDs, while the latter is beneficial for charge separation, which would manifest as an optoelectronic property. Therefore, the as-prepared Phen–DTPA cocrystals integrated merits of both molecular aggregate and charge transfer, endowing them with promising applications in optical and electronic fields.

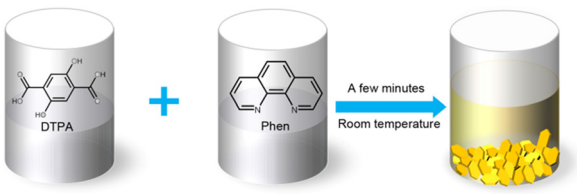

Scheme 1 Schematic diagram of the facile synthesis process of the title Phen–DTPA cocrystal in EtOH solution at room temperature.

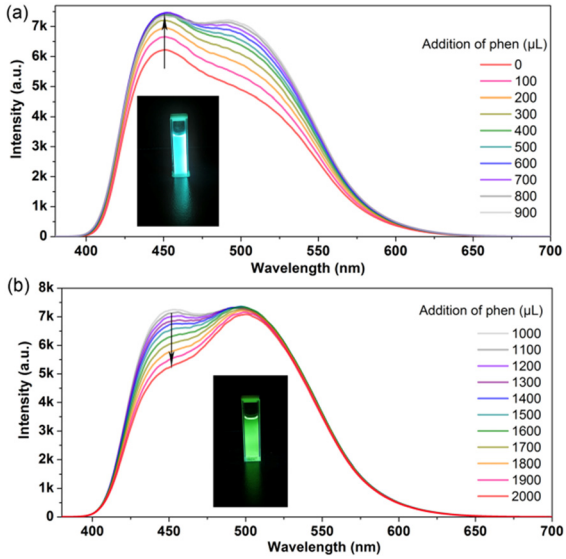

Fig. 1 Fluorescence spectra of DTPA in ethanol (5×10^{-4} M) with the gradual addition of Phen ethanol solution (5×10^{-4} M), showing increase (a) and decrease (b) of the main emission peak at 450 nm. Inserts show the photos of DTPA ethanol solution before and after the addition of Phen under UV light (365 nm) radiation.

Light-yellow layered crystals of Phen–DTPA were synthesized under a fast crystallization process in the ethanol solution at room temperature. The crystal structure and phase purity of the title co-crystal were characterized by single-crystal X-ray diffraction (Table S1†) and powder X-ray diffraction (PXRD, Fig. S2†). The PXRD measurement demonstrates that the powder diffraction peaks measured in the experiments match well with the simulated ones based on the single-crystal diffraction data, supporting the phase purity of the cocrystal sample. The scanning electron microscopy (SEM) images show that the as-synthesized cocrystal particles had a uniformly layered morphology (Fig. S3†). The thermogravimetric analysis (TGA) curve exhibits that the Phen–DTPA cocrystal can be stable up to about 230 °C (Fig. S4†). The FT-IR spectrum (Fig. S5†) reveals the formation of the N–H bond *via* proton transfer at the band of 3056 cm^{-1}. The absorption peak at 1616 and 1332 cm^{-1} can be attributed to asymmetric and symmetric stretching vibrations of a deprotonated carboxylic acid group from DTPA to Phen, respectively.

Single-crystal X-ray diffraction analysis reveals that the title cocrystal Phen–DTPA crystallizes in the triclinic system, $P\bar{1}$ space group with a 1:1 stoichiometry for the two components. Phen–DTPA shows organic salt formed with one proton transferring from the carboxylic group of DTPA to the N atom of Phen. Throughout the process, it still maintained intra-molecular hydrogen bonds between the –OH and COO^- groups of DTPA (Fig. S6†), which are significant for the photophysical properties of the cocrystals.[25] In the structure of Phen–DTPA, the two components are joined together through O–H···O, N–H···O, O–H···N and C–H···O hydrogen bonds. Each DTPA is connected by three DTPA and one Phen (Fig. 2a), whereas each Phen is linked by four DTPA (Fig. 2b).

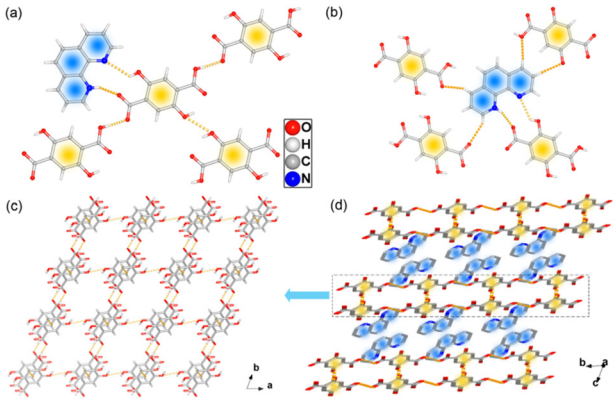

Fig. 2 Hydrogen bond interactions around the DTPA (a) and Phen (b) molecules. (c) View of 2D double-layer structure consists of O–H···O hydrogen bonds and π–π stacking interactions between the DTPA molecules. (d) 3D structure exhibiting alternant arrangement of Phen (blue) and DTPA molecules (yellow).

As for the DTPA molecule, the carboxylic and hydroxy groups are almost co-planar to the phenyl ring due to the above-mentioned intra-molecular hydrogen bonds. The adjacent DTPA molecules are joined together to form a 1D chain along the *b* direction through inter-molecular O–H···O hydrogen bonds (Fig. S7†). The π···π interactions (with a centroid to centroid distance of 3.596 Å) between the phenyl ring of DTPA (Fig. S8†) further extend the chains to a 2D double layer (Fig. 2c and S9†). A view along *a* direction, the overall packing structure of the cocrystal possesses an alternative DADA stacking mode at the molecular level (Fig. 2d). The Phen electronic acceptors are sandwiched between the DTPA 2D double-layer electronic donors.

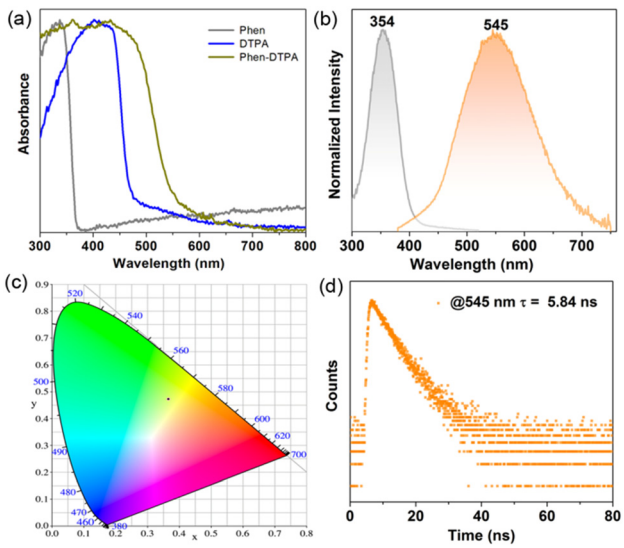

Fig. 3 (a) Normalized UV-vis spectra of Phen, DTPA and Phen–DTPA in the solid state. Normalized excitation/emission spectra (b), CIE-1931 chromaticity diagram (c) and fluorescence decay curve (d) of Phen–DTPA in the solid state measured at room temperature.

The absorption spectra of Phen, DTPA and Phen–DTPA in the solid state are shown in Fig. 3a. Phen and DTPA have absorbance edges approximately at 364 and 473 nm, respectively. On the contrary, the formation of the Phen–DTPA cocrystals can largely extend the absorption band to the visible region in a wide range. The free DTPA and phen in the solid state exhibit a broad emission band and peak at 476 and 362 nm, respectively.[28–30] Upon excitation at 354 nm, Phen–DTPA exhibits a broad fluorescence spectrum with maximum peak at 545 nm (Fig. 3b), quantum yield of 25.8%, and CIE chromaticity coordinates of (0.3647, 0.4735) (Fig. 3c). The decay curve gives a long fluorescence lifetime of 5.84 ns (Fig. 3d). From the above results, it can be concluded that the significant emission red-shift, broad emission spectrum (with a full width at half-maximum of *ca.* 144 nm) and single-exponential decay curve arise from the charge transfer in the D–A cocrystal. Meanwhile, the π···π stacking between the phenyl ring of DTPA can also lead to the bathochromic shift of emission.

To obtain insights into the photophysical properties of the cocrystal, electron density distribution, band structure, and frontier molecular orbital were calculated. The map of the electron density distribution indicates that the electrons are mainly distributed on the two nitrogen atoms of Phen (Fig. S10a†). The electrons in DTPA are occupied by six oxygen atoms (Fig. S10b†). In contrast, strong electrostatic interactions can be observed between the two coformers in the cocrystal. One protonated nitrogen atom in Phen appears electron-deficient state, and the other nitrogen atom and all of the oxygen atoms still exhibit electron accumulation (Fig. 4a). The calculated energy band of 2.181 can correspond to the FL emission peak of Phen–DTPA at 545 nm (Fig. 4b). Frontier orbital analysis shows that isosurface of HOMO is mainly dominated by DTPA (Fig. 4c), whereas the LUMO is exclusively populated on the Phen ligand (Fig. 4d). The

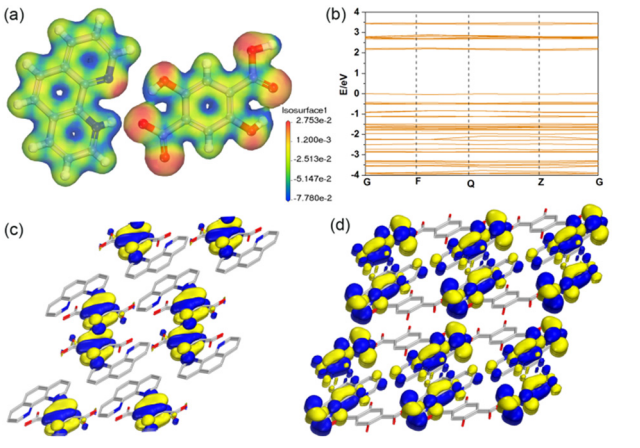

Fig. 4 (a) Electron density distribution of adjacent Phen and DTPA molecules. Red and blue iso-surface present electron accumulation and depletion, respectively. (b) Calculated energy band structure of Phen–DTPA. View of HOMO (c) and LUMO (d) for the profiles based on the DFT calculations of Phen–DTPA.

complete separation of the HOMO–LUMO between Phen and DTPA in the corystal is in favor of charge transfer for photoelectric functional materials.

It is common knowledge that charge transfer materials possess efficient charge separation merit for various optoelectronic applications. The optoelectronic performance of the cocrystal coated on indium tin oxide (ITO) conducting glass (working electrode) was measured in a standard three-electrode system in 0.5 mol L^{-1} Na_2SO_4 aqueous solution. Firstly, the cyclic voltammograms (CV) were obtained in the potential range from −0.6 to 0.6 V (*vs.* Ag/AgCl) at a scan rate of 50 mV s^{-1}. One can see that the weak anode and cathode peak currents appear at about 0.213 V and −0.262 V, respectively, indicating potential electrochemical activity of the Phen–DTPA cocrystal (Fig. 5a). We speculate that the presence of redox peaks may be contributing to the charge transfer between the donor and acceptor. Further linear sweep voltammogram displays that the current density can reach up to −200 μA cm^{-2} with the voltage increasing to −1 V *vs.* Ag/AgCl (Fig. 5b). Radiated by periodical on–off illumination (with a frequency of 10 s), it generates sudden increased photocurrent up to an average peak of −3.56 μA cm^{-2} (I_{light}), and minimum value of −0.005 μA cm^{-2} (I_{dark}) under the dark state (Fig. 5c). This affords a high photocurrent ratio (I_{light}/I_{dark}) of 712, higher than those of pyrene-based MOFs $[Zn(TBAPy)_{1/2}(H_2O)_2]$,[31] $[(HOEtMIm)_2][Mn_3(TBAPy)_2(\mu_2\text{-}OH_2)_2\ (H_2O)_2]$,[32] lower than that of the acridine (AD) based cocrystal complex [AD–TMA],[22] making Phen–DTPA a promising photoelectric detector. By adding a bias potential of −0.5 V under the on–off illumination, a maximum photocurrent of −9.61 μA cm^{-2} was obtained (Fig. S11a†). Electrochemical impedance spectroscopy (EIS) measurements show that the resistance working electrode can be efficiently reduced under light radiation at both 0 V and −0.5 V bias potential (Fig. 5d and S11b†), implying excellent charge transfer performance of Phen–DTPA.

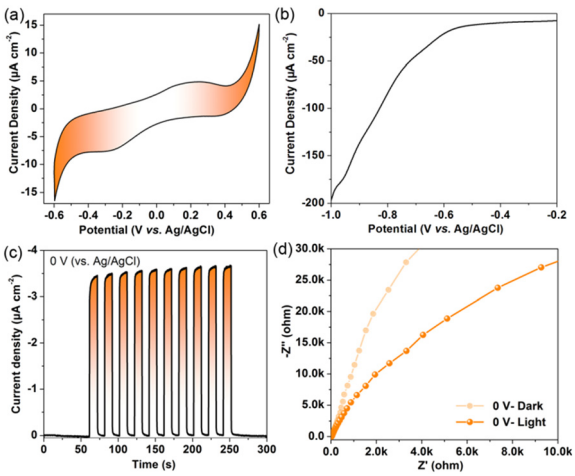

Fig. 5 The cyclic voltammogram (a) and linear sweep voltammogram (b) curves of Phen–DTPA in 0.5 M Na_2SO_4 aqueous solution. (c) Transient current density-time curve of Phen–DTPA without bias potential (0 V). (d) Electrochemical impedance spectroscopy (EIS) Nyquist plots of Phen–DTPA under light and dark states without bias potential (0 V).

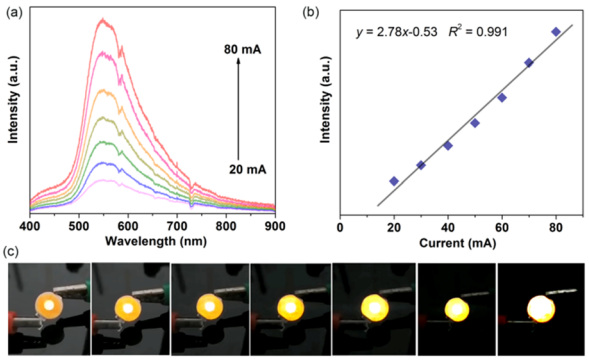

Fig. 6 (a) Fluorescence spectra of Phen–DTPA phosphor-based LED under various drive currents. (b) Relation between the emission intensity and drive current. (c) Photographs of the fabricated LED device under various drive currents (20–80 mA).

By coating the cocrystal powder on a commercial 365 nm diode chip in the presence of epoxy resin as a binder, a phosphor-converted light-emitting diode (LED) device was fabricated. With the increase in the drive current from 20 to 80 mA, the emission intensity of the Phen–DTPA phosphor enhanced gradually (Fig. 6a). During this process, the fluorescence spectra maintained the emission peaks approximately at 547 nm, which are in line with the peak shapes and peak positions of the cocrystal powder's emission spectrum. Meanwhile, the maximum emission intensity *versus* drive current ranging from 20 to 80 mA shows a good linear relationship (Fig. 6b) with a fitted function $y = 2.78x - 0.53$ ($R^2 = 0.991$). Yellow light with different brightness (Fig. 6c) can be observed upon the increase of drive current from 20 to 80 mA. The above results suggest that the title Phen–DTPA cocrystal is a perfect candidate for the solid-state lighting device with high optical performance and stability.

In summary, one new cocrystal complex assembled by 2,5-dihydroxyterephthalic acid (DTPA) donor and 1,10-phenanthroline (Phen) acceptor was successfully prepared using the mixture of ethanolic solutions of the two coformers under a few minutes at room temperature. The combination of experiments and theoretical calculations reveals that the presence of the Phen electric acceptor has a great influence on the stacking mode and electric structure of the DTPA donor, displaying the molecular level of DADA heterojunction in an alternant arrangement mode. The integration of the charge transfer and molecular orbital overlap affords efficient charge separation and high photoluminescent performance for potential photoelectric detectors and LED emitters. Therefore, the present work not only provides an extremely facile and scale-up way to synthesize charge transfer material by co-crystalline engineering but also extends the application of such cocrystals to the field of the photoelectric detector and solid-state lighting.

Conflicts of interest

There are no conflicts to declare.

Acknowledgements

This work was supported by the National Natural Science Foundation of China (No. 22371109, 22171123, 21971100), Science Fund for Distinguished Young Scholars in Henan Province (No. 242300421036).

Notes and references

1 (*a*) K. P. Goetz, H. F. Iqbal, E. G. Bittle, C. A. Hacker, S. Pookpanratana and O. D. Jurchescu, *Mater. Horiz.*, 2022, **9**, 271–280; (*b*) J.-R. Wu, G. Wu, D. Li, M.-H. Li, Y. Wang and Y.-W. Yang, *Nat. Commun.*, 2023, **14**, 5954.

2 (*a*) J. Zhang, J. Jin, H. Xu, Q. Zhang and W. Huang, *J. Mater. Chem. C*, 2018, **6**, 3485–3498; (*b*) K. Liu, Y. Lei and H. Fu, *Chem. Mater.*, 2020, **32**, 5162–5172; (*c*) Y. Wang, C. Wang, J. Zhang, Y. Guo, P. Zhao, X. Fang and G. Zhao, *Chin. Chem. Lett.*, 2023, **34**, 108062; (*d*) K. Wang, Y.-L. Zhu, T.-F. Zheng, X. Xie, J.-L. Chen, Y.-Q. Wu, S.-J. Liu and H.-R. Wen, *Anal. Chem.*, 2023, **95**, 4992–4999.

3 (*a*) J. Han, D. Yang, X. Jin, Y. Jiang, M. Liu and P. Duan, *Angew. Chem., Int. Ed.*, 2019, **58**, 7013–7019; (*b*) S. Ali, P. M. Ismail, M. Khan, A. Dang, S. Ali, A. Zada, F. L. Raziq, I. Khan, M. S. Khan, M. Ateeq, W. Khan, S. H. Bakhtiar, H. Ali, X. Wu, M. I. A. Shah, A. Vinu, J. Yi, P. Xia and L. Qiao, *Nanoscale*, 2024, **16**, 4352–4377; (*c*) Y. Li, B.-L. Chai, H. Xu, T.-F. Zheng, J.-L. Chen, S.-J. Liu and H.-R. Wen, *Inorg. Chem. Front.*, 2022, **9**, 1504–1513; (*d*) J. Li, Y. Zhu, H. Xu, T.-F. Zheng, S.-J. Liu, Y. Wu, J.-L. Chen, Y.-Q. Chen and H.-R. Wen, *Inorg. Chem.*, 2022, **61**, 3607–3615.

4 (*a*) Z. Liang, H. Guo, H. Lei and R. Cao, *Chin. Chem. Lett.*, 2022, **33**, 3999–4002; (*b*) M.-P. Zhuo, Y. Su, Y.-K. Qu, S. Chen, G.-P. He, Y. Yuan, H. Liu, Y.-C. Tao, X.-D. Wang and L.-S. Liao, *Adv. Mater.*, 2021, **33**, 2102719; (*c*) X. G. Yang, J. R. Zhang, X. K. Tian, J. H. Qin, X. Y. Zhang and L. F. Ma, *Angew. Chem.*, 2023, **62**, e202216699.

5 (*a*) S. Cao, L. Song, H. Zhang, J. Han and Y. Zhao, *Chin. Chem. Lett.*, 2023, **34**, 108479; (*b*) H.-X. Bi, X.-Y. Yin, J.-Y. He, H. Song, S.-J. Lu, Y.-Y. Ma and Z.-G. Han, *Rare Met.*, 2023, **42**, 3638–3650; (*c*) J. Ma, R. Sun, K. Xia, Q. Xia, Y. Liu and X. Zhang, *Chem. Rev.*, 2024, **124**, 1738–1861.

6 (*a*) S. K. Park, J. H. Kim, T. Ohto, R. Yamada, A. O. F. Jones, D. R. Whang, I. Cho, S. Oh, S. H. Hong, J. E. Kwon, J. H. Kim, Y. Olivier, R. Fischer, R. Resel, J. Gierschner, H. Tada and S. Y. Park, *Adv. Mater.*, 2017, **29**, 1701346; (*b*) X. G. Yang, Y. J. Chen, P. P. Yin, J. W. Diao, Y. Y. Cheng and L. F. Ma, *Inorg. Chem.*, 2023, **62**, 19389–19394; (*c*) Y.-L. Wu, P.-F. Tang, Q. Zhang, Y.-T. Yan, S. Zhang, G.-P. Yang and Y.-Y. Wang, *Appl. Organomet. Chem.*, 2024, **38**, e7308.

7 A. A. Dar and S. Rashid, *CrystEngComm*, 2021, **23**, 8007–8026.

8 J. Zhang, P. Gu, G. Long, R. Ganguly, Y. Li, N. Aratani, H. Yamada and Q. Zhang, *Chem. Sci.*, 2016, **7**, 3851–3856.

9 G. Bolla, B. Sarma and A. K. Nangia, *Chem. Rev.*, 2022, **122**, 11514–11603.

10 H.-Y. Liu, Y.-C. Lia and X.-D. Wang, *CrystEngComm*, 2023, **25**, 3126–3141.

11 X.-G. Yang, W.-J. Qin, J.-R. Zhang, X.-K. Tian, X. Fan, L.-F. Ma and D. Yan, *Front. Chem.*, 2021, **9**, 765374.

12 S. Singha, R. Jana, R. Mondal, P. P. Ray, P. P. Bag, K. Gupta, N. Pakhira, C. Rizzoli, A. Mallick, S. Kumar and R. Saha, *CrystEngComm*, 2021, **23**, 3510–3523.

13 A. Mandal and B. Nath, *CrystEngComm*, 2022, **24**, 6669–6676.

14 A. N. Manin, K. V. Drozd, A. O. Surov, A. V. Churakov, T. V. Volkova and G. L. Perlovich, *Phys. Chem. Chem. Phys.*, 2020, **22**, 20867–20879.

15 C. Wang, Z. X. You, Y.-H. Xing, F.-Y. Bai and Z. Shi, *CrystEngComm*, 2021, **23**, 4840–4847.

16 Y. Liu, H. Hu, L. Xu, B. Qiu, J. Liang, F. Ding, K. Wang, M. Chu, W. Zhang, M. Ma, B. Chen, X. Yang and Y. S. Zhao, *Angew. Chem., Int. Ed.*, 2020, **59**, 4456–4463.

17 L. Zeng, L. Huang, Z. Wang, J. Wei, K. Huang, W. Lin, C. Duan and G. Han, *Angew. Chem., Int. Ed.*,, 2021, **60**, 23569–23573.

18 Y. Xiao, C. Wu, X. Hu, K. Chen, L. Qi, P. Cui, L. Zhou and Q. Yin, *Cryst. Growth Des.*, 2023, **23**, 4680–4700.

19 S. Li, B. Lu, X. Fang and D. Yan, *Angew. Chem., Int. Ed.*, 2020, **59**, 22623–22630.

20 J.-C. Christopherson, F. Topić, C. J. Barrett and T. Friščić, *Cryst. Growth Des.*, 2018, **18**, 1245–1259.

21 J.-J. Wu, Z.-Z. Li, M.-P. Zhuo, Y. Wu, X.-D. Wang, L.-S. Liao and L. Jiang, *Adv. Opt. Mater.*, 2018, **6**, 1701300.

22 X.-G. Yang, Z.-M. Zhai, X.-M. Lu, L.-F. Ma and D. Yan, *ACS Cent. Sci.*, 2020, **6**, 1169–1178.

23 L. Sun, W. Hua, Y. Liu, G. Tian, M. Chen, M. Chen, F. Yang, S. Wang, X. Zhang, Y. Luo and W. Hu, *Angew. Chem., Int. Ed.*, 2019, **58**, 11311–11316.

24 K. Jayaramulu, P. Kanoo, S. J. George and T. K. Maji, *Chem. Commun.*, 2010, **46**, 7906–7908.

25 E. Papazoi, A. Douvali, S. A. Diamantis, G. S. Papaefstathiou, S. V. Eliseeva, S. Petoud, A. G. Hatzidimitriou, T. Lazarides and M. J. Manos, *Mol. Syst. Des. Eng.*, 2020, **5**, 461–468.

26 X. Yan, J. Lei, Y.-P. Li, P. Zhang, Y. Wang, S.-N. Li and Q.-G. Zhai, *CrystEngComm*, 2022, **24**, 2264–2269.

27 D. J. Vogel, T. M. Nenoff and J. M. Rimsz, *ACS Appl. Mater. Interfaces*, 2020, **12**, 4531–4539.

28 X.-G. Yang, X.-M. Lu, Z.-M. Zhai, J.-H. Qin, X.-H. Chang, M.-L. Han, F.-F. Li and L.-F. Ma, *Inorg. Chem. Front.*, 2020, **7**, 2224–2230.

29 L. Dun, B. Zhang, J. Wang, H. Wang, X. Chen and C. Li, *Crystals*, 2020, **10**, 1105.

30 J. Fu, J. Gu, Z. Bao, Y. Zhou, H. Hu, C. Yang, R. Wu, H. Liu, L. Qin, H. Xu, J. Li, H. Guo, L. Wang, Y. Zhou, X. Wang and G. Li, *Anal. Chem.*, 2023, **95**, 18709–18718.

31 J.-H. Qin, Y.-D. Huang, Y. Zhao, X.-G. Yang, F.-F. Li, C. Wang and L.-F. Ma, *Inorg. Chem.*, 2019, **58**, 15013–15016.

32 X.-G. Yang, J.-H. Qin, Y.-D. Huang, Z.-M. Zhai, L.-F. Ma and D. Yan, *J. Mater. Chem. C*, 2020, **8**, 17169–17175.

